Fermi National Accelerator Laboratory

FERMILAB-Pub-76/65-EXP
7100.096

(Submitted to Phys. Rev.)

IMPACT PARAMETER ANALYSIS OF ELASTIC SCATTERING FROM 50 TO 175 GeV/c

D. S. Ayres and R. Diebold
Argonne National Laboratory, Argonne, Illinois 60439

D. Cutts, R. E. Lanou, L. J. Levinson, and J. T. Massimo
Brown University, Providence, Rhode Island 02912

J. Litt and R. Meunier
CERN, Geneva, Switzerland

M. Sogard, B. Gittelman, and E. C. Loh
Cornell University, Ithaca, New York 14850

A. E. Brenner, J. E. Elias, and G. Mikenberg
Fermi National Accelerator Laboratory, Batavia, Illinois 60510

L. Guerriero, P. Lavopa, G. Maggi, C. DeMarzo,
F. Posa, G. Selvaggi, P. Spinelli, and F. Waldner
Istituto Nazionale di Fisica Nucleare, Sezione di Bari, Italy

D. S. Barton, J. Butler, J. Fines, J. I. Friedman,
H. W. Kendall, B. Nelson, L. Rosenson, and R. Verdier
Massachusetts Institute of Technology, Cambridge, Massachusetts 02139

B. Gottschalk
Northeastern University, Boston, Massachusetts 02115

and

R. L. Anderson, D. Gustavson, K. Rich, D. M. Ritson, and G. A. Weitsch
Stanford Linear Accelerator Center, Stanford, California 94305

July 1976

FERMILAB-Pub-76/65-EXP

IMPACT PARAMETER ANALYSIS OF ELASTIC SCATTERING FROM 50 TO 175 GeV/c*

D. S. Ayres and R. Diebold
Argonne National Laboratory, Argonne, IL 60439
D. Cutts, R. E. Lanou, L. J. Levinson, and J. T. Massimo
Brown University, Providence, RI 02912
J. Litt† and R. Meunier††
CERN, Geneva, Switzerland
M. Sogard***, B. Gittelman and E. C. Loh**
Cornell University, Ithaca, NY 14850
A. E. Brenner, J. E. Elias and G. Mikenberg
Fermi National Accelerator Laboratory, Batavia, IL 60510
L. Guerriero, P. Lavopa, G. Maggi, C. DeMarzo,
F. Posa, G. Selvaggi, P. Spinelli and F. Waldner
Istituto Nazionale di Fisica Nucleare, Sezione di Bari, Italy
D. S. Barton, J. Butler****, J. Fines, J. I. Friedman,
H. W. Kendall, B. Nelson, L. Rosenson and R. Verdier
Massachusetts Institute of Technology, Cambridge, MA 02139
B. Gottschalk
Northeastern University, Boston, MA 02115
R. L. Anderson, D. Gustavson, K. Rich, D. M. Ritson and G. A. Weitsch†††
Stanford Linear Accelerator Center, Stanford, CA 94305

ABSTRACT

Impact parameter representations of elastic differential cross sections for the processes $\pi^{\pm}p$, $K^{\pm}p$ and $p^{\pm}p$ at incident energies from 50 GeV to 175 GeV and in the $-t$ range 0.03 GeV^2 to 0.75 GeV^2 are presented. The meson-baryon interactions are found to be 20% more transparent, with an interaction radius 6% smaller than the baryon-baryon interaction. The increase in the p-p total cross section as a function of energy is shown to come primarily from an increase in the p-p interaction radius, while in the K^+p case, an increase is seen in both the central opacity and the interaction radius.

*Work supported in part by the U. S. Energy Research and Development Administration, the National Science Foundation and Istituto Nazionale di Fisica Nucleare (Italy).

**Current address: University of Utah, Salt Lake City, Utah 84112
***Current address: University of Chicago, Chicago, Illinois 60637
****Current address: University of Illinois, Champaign/Urbana, Illinois 61801
†Current address: Daresbury Nuclear Physics Laboratory, Daresbury, Lancashire, England
††Also at: Centre d' Etudes Nucléaire de Saclay, 91 Gif-sur-Yvette, France
†††Current address: Centre d' Etudes Nuclearie de Saclay, 91 Gif-sur-Yvette, France

I. Introduction

With the discovery of the dip at $t \simeq -1.4$ GeV^2 in pp elastic scattering[1] and the measurements of the real part of the elastic amplitude at $t=0$[2] in the Fermilab-ISR energy range, it became apparent that the elastic scattering amplitude can be considered, to a good approximation, to be purely imaginary at high energies. This fact has enabled several authors [3-6] to perform a transformation of the pp elastic amplitude to impact parameter space, and further, to obtain the total and inelastic cross sections as a function of impact parameter making use of the fact that the S-matrix is diagonal in impact parameter space. The observed increase in the inelastic and total cross sections as a function of energy for pp collisions was found to be peripheral and centered at an impact parameter, b, of approximately 1 Fermi[3-6]. The Pumplin bound[7] for inelastic diffraction was also obtained, and the implications were that inelastic diffraction is more peripheral than the elastic process.

This paper presents the results of an impact parameter analysis of the elastic reactions $\pi^{\pm}p$, $K^{\pm}p$ and $p^{\pm}p$ for incident momenta from 50 GeV/c to 175 GeV/c and for $-t$ in the range 0.03 to 0.75 GeV^2, obtained with the Fermilab Single Arm Spectrometer in the M6E beam line, that has been described in a previous publication[8]. Similar analyses have been done on preliminary data[9] and the results are consistent with those included in this publication. In the next section a discussion of the method used to transform the elastic data to impact parameter space and the error calculation for this procedure is presented. In Section III, the general characteristics of the different reactions in impact parameter space, including their energy dependence are discussed. In Section IV, the observed increase in the total and inelastic K^+p and pp cross sections is correlated with changes in the impact parameter distributions. Sections V contains results on the upper limits for inelastic diffraction as a function of impact parameter. The peripherality of ω exchange has been discussed in connection with low energy $K^{\pm}p$ data[10], and in Section VI those conclusions are extended to the Fermilab energy range. In Section VII the hadronic matter distributions for π, K and p as calculated using the Chou-Yang model

are compared with electromagnetic form factor measurements. In Section VIII comparisons with Quark Model predictions as viewed in impact parameter space are shown. Conclusions are presented in the final section.

II. Elastic Cross Sections and Transformation Method

The results from the Fermilab Single Arm Spectrometer on the differential elastic cross sections for the processes $\pi^{\pm}p$, $K^{\pm}p$ and $p^{\pm}p$ have been published previously[8], and can all be satisfactorily fit by the parameterization:

$$d\sigma/dt = Ae^{Bt+Ct^2} \qquad (1)$$

for $-t \leq 0.75 GeV^2$. The uncertainty in the overall normalization is ±3%. Figure 1 shows the ratio of the parameter A as obtained from the fits to the optical point values derived from the total cross section measurements[11]. With the exception of $\bar{\pi}p$ at 50 GeV/c, all values are within one standard deviation of unity, and therefore, the optical point was included in the data with a 3% uncertainty. Since the measurements are consistent with other parametrizations, such as piecewise exponentials with a break at $-t=0.15$ GeV^2 or the sum of two exponentials, the transformation to impact parameter space has been made in numerical form, and therefore in a parametrization independent way.

The impact parameter representation, $h_{el}(s,b)$, of the elastic amplitude is defined by its Fourier transform. After integrating over the angular dependence the transformation reduces to a convolution integral of the elastic amplitude and the J_o Bessel function. The method used to perform the transformation was to calculate for each data point $d\sigma/dt(t_i)=d\sigma/dt_i$ and its corresponding Δt_i interval, the quantities:

$$h_i(b) = \left(\frac{1}{4\pi}\right) e^{B_{eff}^{i}|t_i|/2} \sqrt{\frac{d\sigma}{dt_i}} \int_{\Delta t_i} e^{-B_{eff}^{i}|t|/2} J_o(b\sqrt{-t})\, dt \qquad (2)$$

$$\Delta h_i(b) = \left(\frac{1}{4\pi}\right) e^{B_{eff}^{i}|t_i|/2} \Delta\sqrt{\frac{d\sigma}{dt_i}} \int_{\Delta t_i} e^{-B_{eff}^{i}|t|/2} J_o(b\sqrt{-t})\, dt \qquad (3)$$

where B^i_{eff} is the logarithmic slope $d(\ln d\sigma/dt)/dt$ given by the parametrization (1) at the value t_i, and $\Delta\sqrt{(d\sigma/dt_i)}$ is the statistical error on $\sqrt{d\sigma/dt_i}$. Finally, $h_{el}(s,b) = \sum_i h_i(b)$ and $\Delta h_{el}(s,b) = \sqrt{\sum(\Delta h_i(b))^2}$ are calculated for each b and s value and for all six reactions. The function $h_{el}(s,b)$ was found to be independent of the value taken for B^i_{eff}, for b values smaller than 1.8 Fermi. For example, by taking 5 x B^i_{eff} for the transformation, identical results (to within 1%) for $h_{el}(s,b)$, $b \leq 1.8$ Fermi were obtained and therefore $\Delta h_{el}(s,b)$ represents the error in the transformation.

The unitarity equation in impact parameter space is:

$$\text{Im } h_{el}(s,b) = \tfrac{1}{4}|h_{el}(s,b)|^2 + G_{inel}(s,b) \qquad (4)$$

where the different terms are related to the total, elastic and inelastic cross sections as follows:

$$d\sigma_{tot}/\pi db^2 = \text{Im. } h_{el}(s,b),$$

$$d\sigma_{el}/\pi db^2 = \tfrac{1}{4} \mid h_{el}(s,b)|^2,$$

$$d\sigma_{inel}/\pi db^2 = G_{inel}(s,b). \qquad (5)$$

To use equation (4), a knowledge of the real and imaginary part of $h_{el}(s,b)$ is needed. Since the real part of the elastic amplitude can only be measured in the Coulomb interference region, a model must be used to estimate the real part of $h_{el}(s,b)$.

Figure 2 shows the decomposition of $h_{el}(s,b)$ for π^+p at 50 GeV/^{2} as an example, into the contribution from various t regions. The main contribution comes from the region $-t \leq 0.15$ GeV^2 where in terms of the elastic amplitude A(t), the measured ratios $\rho(t) = \text{Re}A(t)/\text{Im}A(t)$ can be used. The Coulomb interference measurements[2] give $\rho(0) \leq 0.15$ for all processes in our energy range and therefore the real part contribution to $h_{el}(s,b)$ from the small -t region is less than 1%. Interpreting the dip at $t=-1.4$ GeV^2 in pp elastic scattering at ISR as a zero of the imaginary part of the elastic amplitude[3], an estimate of the real part at $t \neq 0$ can be made by using a linear extrapolation for $1/\rho(t)$ from the measured $\rho(0)$ value. In πp and Kp

scattering such a dip is not seen at Fermilab[12] energies and can therefore be assumed to occur at larger -t values giving a smaller value for $1/\rho(t)$ slope. The real part contributions to $h_{el}(s,b)$ from the regions $0.15 \leq -t \leq 0.4$ GeV^2 and $0.4 \leq -t \leq 0.75$ GeV^2 calculated by taking twice the $\rho(t)$ value predicted by the linear extrapolation are each less than 2%. The procedure is comparable to allowing the Pomeron slope to be as large as 0.6 GeV^{-2}. Finally, the different t regions contribute to $h_{el}(s,b)$ with different signs and produce a partial cancellation of the real part. Therefore, the conclusion is that the overall error in the assumption

$$\text{Im } h_{el}(s,b) = h_{el}(s,b) \qquad (6)$$

is less than 3%.

Since the impact parameter representation of the elastic amplitude is obtained by integrating over all t values, the contributions to $h_{el}(s,b)$ from $-t \geq 0.75$ GeV^2 had to be estimated. The data taken at $P_{lab} = 100$ GeV extended out to $-t = 1.4$ GeV^2 and was used to estimate the large -t contributions at other energies. The ratio

$$\frac{h_{el}(b, \text{ for } -t \leq 1.4 \text{ GeV}^2)}{h_{el}(b, \text{ for } -t \leq .75 \text{ GeV}^2)} = 1 + C^{xp}(b) \qquad (7)$$

was calculated for the reactions $pp \to pp$ and $\pi^{\pm} p \to \pi^{\pm} p$. This ratio is 1 for $b > 0.2$ Fermi, and is equal to 1.02 and 1.06 at $b \approx 0$ for pp and πp respectively. Since the real part of the elastic amplitude becomes comparable to imaginary part for $-t \geq 0.75$ GeV^2, the impact parameter representation has been corrected by taking half of the large $|t|$ correction,

$$\text{Im } h_{el}(s,b) = h_{el}\left[s, b, -t \leq 0.75 \text{ GeV}^2\right] \quad (1 + \tfrac{1}{2} C^{xp}(b)) \qquad (8)$$

where $C^{pp}(b)$ was used for $p^{\pm}p$ and $C^{\pi^{\pm}p}(b)$ was used for $\pi^{\pm}p$ as well as $K^{\pm}p$. An uncertainty of $\frac{1}{2} C^{xp}(b)$ was included for this procedure. An additional uncertainty for $b \leq 0.1$ Fermi is due to the contributions from $-t \geq 1.4$ GeV^2. Because of the lack of data in meson-baryon elastic scattering at high $|t|$ in this energy range, and the uncertainties in the

real parts at large $|t|$ values, this correction cannot be directly determined but has been estimated to be less than 3% for the meson-baryon cas and 1% for the baryon-baryon case.

III. General Characteristics

Figure 3 shows the imaginary part of the elastic amplitude as defined in equation (8) as a function of impact parameter for all reactions at P_{lab}=50 and 175 GeV/c. The errors shown include the uncertainty in the correction for the contribution in the region $0.75 \leq |t| \leq 1.4$ Gev^2. The following conclusions can be reached:

a) $\pi^{\pm}p$ and K^-p show almost no change as a function of energy,

b) K^+p shows a slight increase as a function of energy for all b values,

c) $\bar{p}p$ shows a slight decrease as a function of energy for all b values within the uncertainties of this analysis,

d) in pp there is a decrease in Im. $h_{el}(s,b)$ for small b and an increase for large b values as a function of energy.

Figure 4 shows the values of Im. $h_{el}(s,b=0)$ as a function of s for the various processes. The errors also include the estimated error incurred by neglecting the real part of the elastic amplitude. The relative errors are much smaller since neither the real part nor the large $|t|$ cross section change very strongly in our energy range.

By making use of the unitarity equation (4), one can calculate the inelastic cross section $G_{inel}(s,b) \equiv d\sigma_{inel}/\pi db^2$ as a function of b. The value of this cross section at b=0 is shown for all processes in Figure 5 with the full errors included as for the plots in Figure 4. For comparison, the results of similar calculations done for pp with ISR data and a 24 GeV/c experiment[3] are included. Since $G_{inel}(s,b=0)$ represents the absorption probability for a head-on collision, the results show that a baryon has a ~6% probability of colliding head-on with a proton without any absorption, while this probability is ~18% for pions and ~25% for kaons. As one can see, mesons are very transparent objects.

Figures 6a and 6b show the RMS interaction distance for the total and inelastic cross sections, defined by

$$\sqrt{R_i^2} = \left[\int_0^{b_{max}} b^2 (d\sigma_i/db^2) b db \Big/ \int_0^{b_{max}} (d\sigma_i/db^2) b db \right]^{1/2} \qquad (9)$$

where i=total, inelastic, and b_{max} was taken to be 1.6 Fermi. For $b \geq 1.6$ Fermi the impact parameter transformation becomes very sensitive to the $d\sigma/dt$ parametrization used between t=o and the minimum $|t|$ value measured. By taking b_{max} = 2 Fermi, the values of $\sqrt{R^2_{total}}$ changes by 12% for all reactions, but the results for $K^{\pm}$ and $\bar{p}$ present large fluctuations (~5%) as a function of energy. With the exception of the $\bar{p}p$ process both the total and inelastic processes are consistent with an increase in the RMS interaction radius with s. The total and inelastic interaction radii for the meson-baryon interactions are 6% smaller than the baryon-baryon interaction radii.

IV. Total Cross Section Increase in K^+p and pp.

The only total cross sections that show a definite increase in the energy range under study are K^+p (~7%) and pp (~1%)[11]. However, when a 7% difference is spread over b-space the average contribution to this difference is smaller than the error bars. Assuming that both the real parts and the large $|t|$ contributions do not change by more than 2% within this energy range, the differences can sensibly be plotted including only the statistical errors.

Figures 7a and 7b show plots of the differences

$$\Delta\left(\frac{1}{\pi}\frac{d\sigma_{tot}}{db^2}\right)_{P_1,P_2} = \frac{1}{\pi}\frac{d\sigma_{tot}(P_1)}{db^2} - \frac{1}{\pi}\frac{d\sigma_{tot}(P_2)}{db^2} \qquad (10)$$

for P_1=175 Gev/c, P_2=70 GeV/c and P_1=140 GeV/c, P_2=50 GeV/c($P_i \equiv P_{lab_i}$) for the processes pp and K^+p respectively. The two pairs of P_1, P_2 values were chosen in such a way that the two cross section differences are equal[11] to within 1%, and therefore, the two graphs can be compared and also averaged. The two process appear to be different.

For pp, $d\sigma_{tot}/\pi db^2$ is decreasing at small b values and increasing at large b values indicating a peripheral increase in the total cross section. For the K^+p case, the total cross section distribution seems to be increasing at small b values and therefore is consistent with a non-peripheral increase in the cross section.

Since this part of the analysis is speculative in nature, we have proceeded one step further to isolate the Pomeron from f exchange in impact parameter space. This is done by looking at the SU(3) combination which isolates the Φp total cross section:

$$\frac{d\sigma_{tot}(\Phi p)}{\pi db^2} = \frac{d\sigma_{tot}(K^+p+K^-p)}{\pi db^2} - \frac{d\sigma_{tot}}{2\pi db^2}(\pi^+p+\pi^-p) \qquad (11)$$

If the f trajectory is neglected due to its low intercept, the Φp total cross section as defined in (11) isolates Pomeron exchange. Indeed, by taking the above SU(3) combination, a total cross section for Φp is obtained that increases logarithmically[13] from P_{lab}=6 GeV/c to P_{lab}=200 GeV/c. In Figure (7b), $\Delta(d\sigma_{tot}/\pi db^2)$ as defined in (10) for P_1=175 and P_2=70 GeV/c is plotted for the Φp process. In contrast to the pp case the increase in the total Φp cross section is non-peripheral and similar to the K^+p behavior.

In Figures 8a and 8b the differences in the inelastic cross sections are plotted for the same P_1, P_2 values as before. For a comparison, the average values for the two sets of total cross sections differences in Figures 7a and 7b have also been plotted and are shown as a dash-dot curve. Since the difference between the total and inelastic cross sections is the elastic cross section, one concludes that most of the total cross section decrease at small b values for pp comes from the elastic cross section decrease, while the large b increase comes mainly from an increase in the inelastic cross section.

V. Upper Limits on Inelastic Diffraction

There have been various recent theoretical works over the close interdependence between elastic and inelastic diffraction[14]. Pumplin[7] has shown that s-channel unitarity combined with the assumption that inelastic as well as elastic diffraction is the shadow of non-diffractive particle production implies the following upper bound on inelastic diffraction.

$$\frac{1}{\pi}\frac{d\sigma_{diff}}{db^2} \leq \frac{1}{2\pi}\frac{d\sigma_{tot}}{db^2} - \frac{1}{\pi}\frac{d\sigma_{el}}{db^2} \equiv \sigma^{max}_{diff}(b) \qquad (12)$$

In Figure 9, we present a plot of $\sigma^{max}_{diff}(b)$ for all processes at P=175 GeV/c (the plots at other energies look similar) and for comparison we plot $d\sigma_{el}/\pi db^2$ for each reaction at 50 GeV/c and 175 GeV/c. The salient feature of those plots is that the $\sigma^{max}_{diff}(b)$ profile is peripheral for $p^{\pm}p$ in contrast to the more central meson-baryon scattering profiles. However, they are more peripheral than the corresponding elastic profiles.

Experimental results on total inelastic diffraction for pp and πp have been shown [14] to be consistent with the relation $\sigma^{diff}_{inel} \approx \sigma_{elast}$. The fact that the elastic contribution at b=0 is three times the Pumplin bound for pp inelastic diffraction scattering implies that inelastic diffraction has a larger RMS interaction radius than the elastic pp process. However, this is not the case for the meson-baryon process where the elastic contribution at b=0 is approximately equal to the Pumplin bound, and, therefore, no such conclusion is possible.

VI. Regge Contributions

The cross overs between particle and anti-particle elastic cross sections for K^-p, K^+p and $\bar{p}p$, pp have been studied in lower energy elastic scattering experiments[15]. The cross overs have also been observed at high energies[16]. These differences have been explained in terms of dual models[10] by using the fact that K^+p and pp are exotic in the s channel so that only pomeron exchange contributes. Further, the Regge contributions to K^-p and $\bar{p}p$ are small when compared with the Pomeron part and only the interference term between the Pomeron term and the imaginary (Regge) term is important for the cross over. The results of these theoretical analyses[10] show that the imaginary part of the odd-charge-conjugation Regge exchange amplitude, ω exchange in this case, has an $e^{Bt}J_o(R\sqrt{-t})$ behavior that corresponds in impact parameter space, to a distribution peaking at b=R.

Presented in Figures 10a and 10b are the differences

$$\Delta\sigma_{tot}^{xp}(b) \equiv \frac{d\sigma_{tot}(x^-p)}{\pi db^2} - \frac{d\sigma_{tot}(x^+p)}{\pi\, db^2} \qquad (13)$$

for x=K and p respectively at P_{lab}=50 and 175 GeV/c. In both cases there is an indication of a peak which decreases as a function of energy. The peak occurs at b~0.9 Fermi for Kp and b~1.2 Fermi for pp. One may conclude that the amount of non-flip ω exchange is very small in K^-p, consistent with zero at P_{lab}=175 GeV/c, and is significant for $\bar{p}p$ at 50 GeV/c , but decreases very fast to a small contribution at P_{lab}=175 GeV/c.

VII. Hadronic Density Distributions in K, π and p

Chou and Yang[17] have defined a hadronic density distribution (or density of opaqueness) by assuming that the attenuation of the probability amplitude, S(b), for a scattering process between two hadrons is governed by the local density (opaqueness) within each hadron. In a mathematical form the above assumption would read for the scattering of particle a on b

$$-\ln(1-\mathrm{Imh}_{el}(s,b)) = -\ln S(b) = \mathrm{Const}\int\int D_a(\vec{b}-\vec{b}')D_b(\vec{b}')\, d^2b' \qquad (14)$$

where $D_i(\vec{b})$ is a two-dimensional hadronic density defined by integrating the hadronic density along the direction of the incoming particle.

Denoting the Fourier transform of A by $\langle A\rangle$, then the Fourier transform of (14) would read:

$$\langle -\ln(1-\mathrm{Imh}_{ei}(s,b))\rangle = \mathrm{Const}\,\langle D_a(b)\rangle\langle D_b(b)\rangle \qquad (15)$$

Using the pp data to determine $\langle D_p(b)\rangle$, the results can then be inserted in (14) for the πp and Kp processes to obtain $\langle D_\pi(b)\rangle$ and $\langle D_K(b)\rangle$.

Chou and Yang[17] have suggested that the Fourier transform of the hadronic density should be compared with the Fourier transform of the hadronic charge distribution obtained from electron scattering measurements. Such a comparison is performed in Figure 11 for protons and pions. In the proton case, the comparison is not well defined since the proton has two electromagnetic form factors, electric and magnetic. For that reason the comparison shown in Figure 11a is done with both F_1 and G_E as obtained by Price et el[18]. At low energy, good agreement with F_1 is experimentally obtained while for the ISR range the agreement with G_E is better[19]. In the case of the π form factor, there is data on πe scattering only for $|t|\leq 0.04$ GeV^2 (2 and the high $|t|$ data points are obtained from electroproduction of pions[21]. The agreement of $\langle D_\pi(b)\rangle$ with the pion form factor, as shown in Figure 11b, is excellent and therefore it is tempting to predict how the K form factor (the dotted line in Figure 11b) will look on the basis of this model.

VIII. Quark Model Predictions

Various differences between meson-baryon and baryon-baryon scattering have been shown. Since those processes are related in terms of quark counting in a simple quark model, a comparison between πp, Kp and pp amplitudes in terms of those predictions will be given.

Figures 12a and 12b show the differences $3/2W(\pi p) - W(pp)$ $W(\pi p)-W(Kp)$ respectively, where:

$$W(xp)= \frac{1}{2\pi} \frac{d\sigma_{tot}}{db^2} (x^+p) + \frac{1}{2\pi} \frac{d\sigma_{tot}}{db^2} (x^-p) \qquad (16)$$

for P_{lab}=50, 175 GeV/c. The prediction of quark counting is that those differences should be zero. However, due to the fact that $3/2(Imh_{el}^{\pi p}(s,b=0) > Imh_{el}^{pp}(s,b=0)$ and that the interaction radius is different for πp and pp, the difference oscillates around zero in the first case. In the second case, the fact that Kp is more transparent than πp makes the difference larger than zero. Since elastic scattering contains other exchanges besides vacuum quantum numbers, Lipkin has suggested a quark model relation that takes into account f exchange[22]. This relation is plotted in Figure (13) and even though it is ~7% different than unity, it is quite constant for b <1 Fermi.

IX. Conclusions

It has been shown that the impact parameter representation provides a very useful tool to analyze hadronic interactions at high energies since it interrelates elastic and inelastic physics in a very natural way.

The following general conclusions can be drawn from the analysis presented on the impact parameter representation of elastic scattering data obtained with the Fermilab Single Arm Spectrometer:

a) Meson-baryon interactions are ~20% more transparent than baryon-baryon interactions, which approach an opacity of 94% for S>200Gev^2.

b) Meson-baryon processes have an interaction radius ~6% smaller than baryon-baryon processes.

c) The decrease with energy of the $\bar{p}p$ elastic cross section at large b values (b ~1 Fermi) is correlated with the decrease of C=-1 (non-Flip ω) Regge exchanges, while the decrease at small b values is common to both pp and $\bar{p}p$ elastic cross section and is produced by a different mechanism.

d) The increase in the pp total cross section as a function of energy is peripheral while in the K^+p case this increase could also be central.

e) The Pumplin upper limit for inelastic diffraction requires $p^{\pm}p$ inelastic diffraction to be more peripheral than the elastic process but imposes only very small restrictions in the meson-baryon case.

f) The Fourier transform of the π hadronic density is found to be in excellent agreement with the π form factor measurements.

g) The results of the analysis disagree with the simple quark model counting.

Ackknowledgement

We would like to thank Drs. E. Rabinovici and U. Maor for their very stimulating discussions. We would also like to express our thanks to the many people at our home institutions and at Fermilab who have contributed to the successful operation of the Single Arm Spectrometer.

References

1. A. Bohm et al., Phys. Lett. B49, 491 (1974).
2. V. Bartenev et al., Phys. Rev. Lett. 31, 1367 (1974).
   U. Amaldi et al., Phys. Lett. 43B, 231 (1973). See also J. Lach, Fermilab preprint CONF-76/15.
3. H. I. Miettinen, CERN preprint TH.1864, 1974.
4. R. Henzi and P. Valin, Phys. Lett. B48, 119 (1974).
5. F. S. Henyey et al., Nuclear Physics B70, 445 (1974).
6. A. W. Chao and C. N. Yang, Phys. Rev. D8, 2063 (1973).
7. J. Pumplin, Phys. Rev. D8, 2899 (1973); see also
   R. Blankenbecler et al., Phys. Rev. D9, 736 (1974).
8. Fermilab Single Arm Spectrometer Group, Phys. Rev. Lett. 35, 1195 (1975).
   and D. S. Ayres, et al, to be published.
9. J. Butler, M.I.T., Ph.D. Thesis, 1975, unpublished.
   D. Cutts and B. Heltsley, Brown University internal reports 135 (COO-313-TB-219) and 137 (COO-3130TB-221).
   G. Mikenberg, J. Butler and D. Cutts, Bulletin of the American Physical Society, 21, 669 (1976).
10. M. Davier and H. Harari, Phys. Lett. B40, 281 (1972).
11. A. S. Carroll et al., Phys. Rev. Lett. 33, 928 (1974).
12. C. W. Akerlof et al., Phys. Rev. Let. (1975).
13. C. Quigg and E. Rabinovici, Fermilab preprint 75/81-THY(1975).
14. K. Fiakowski and H. I. Miettinen, CERN preprint Th.2057 (1975).
15. I. Ambats et al., Phys. Rev. D9, 1179 (1974); see also
    G. Brandenburg et al., Phys. Lett. B58, 367 and 371 (1975).
16. R. L. Anderson, et al., submitted to Phys. Rev. Lett.
17. T. T. Chou and C. N. Yang, Phys. Rev. 170, 1591 (1968).
18. L. E. Price et al., Phys. Rev. D4, 45 (1971).
19. A. W. Chao and C. N. Yan, Phys. Rev. D8, 2063 (1973).
20. G. T. Adylov et al., Phys. Letters 51B, 402 (1974).
21. C. J. Bebek et al., Phys. Rev. D13, 25 (1976).
22. H. J. Lipkin, Phys. Letters B56, 76 (1975).

Figure Captions

Figure 1 The ratio of parameter A, as obtained from the fits to equation (1) to the optical point values as calculated from σ_{total} given by Reference 11 and corrected for the real part using the results given in Reference 2 for the elastic reactions $\pi^{\pm}p$, $K^{\pm}p$, and $p^{\pm}p$.

Figure 2 $h_{el}(s,b)$ for $\pi^{+}p$ at 50 GeV/c in arbitrary units for the integration ranges indicated.

Figure 3 Im $h_{el}(s,b)$ for the reactions $\pi^{\pm}p$, $K^{\pm}p$, and $p^{\pm}p$ at 50 GeV/c(●) and at 175 GeV/c(x). The errors shown include both the statistical errors and the uncertainty due to corrections for the large $|t|$ contributions and the real part effects.

Figure 4 Im $h_{el}(s,b=0)$ as a function of s for $\pi^{\pm}p$, $K^{\pm}p$ and $p^{\pm}p$. The errors are calculated as for Figure 3.

Figure 5 $G_{inel}(s,b=0)$ as a function of s for $\pi^{\pm}p$, $K^{\pm}p$ and $p^{\pm}p$. The errors are calculated as for Figure 3. The ISR and 24 GeV/c points in pp are included as given in Reference 3.

Figure 6 The RMS interaction distances for (a) the total and (b) the inelastic cross sections as a function of s for $\pi^{\pm}p$, $K^{\pm}p$ and $p^{\pm}p$. The errors are calculated as for Figure 3.

Figure 7 $\Delta(d\sigma_{tot}/\pi db^2)$ for pp (a) and $K^{+}p$ (b) with P_1=175, P_2=70 GeV/c (o) and P_1=140, P_2=50 GeV/c(□). In 7b the difference for ϕp at P_1=175, P_2=70 GeV/c is also plotted as (x).

Figure 8 $\Delta(d\sigma_{inel}/\pi db^2)$ for pp (a) and $K^{+}p$ (b) with P_1 and P_2 as in Figure 7. The broken line is the average of the two curves presented in Figure 7.

Figure 9 $\sigma_{diff}^{max}(b)$ for $\pi^{\pm}p$, $K^{\pm}p$ and pp at P=175 GeV/c(solid line) and $d\sigma_{elast}/\pi db^2$ at 50 GeV/c(x) and at 175 GeV/c(●).

Figure 10 $\Delta\sigma_{tot}^{xp}(b)$ for (a) Kp and (b) pp at P=50 GeV/c(o) and at P=175 GeV/c (x).

Figure 11(a) F_1^p (t) (●) and G_E^p (t) (○) proton form factors from Reference 18. The solid line corresponds to the calculated $\langle D_p(b) \rangle$ using equation (14) for pp scattering 175 GeV/c, normalized to $\langle D_p(b) \rangle = 1$, at t=0.

(b) Pion form factor measurements from Reference 19 (●) and Reference 20 (○,□). In the region of this measurement, the solid (dotted) line corresponds to the Fourier transform of the pion (Kaon) hadronic density calculated using (14) for $\pi^+ p$ ($K^+ p$) and pp scattering at 175 GeV/c, normalized to $\langle D_\pi(b) \rangle = 1$ ($\langle D_K(b) \rangle = 1$), at t=0.

Figure 12 Quark model comparisons at P=50 GeV/c (●) and at P=175 GeV/c(x).

Figure 13 Quark model, modified for f exchange, comparison for P=50 GeV/c (●) and P=175 GeV/c (x).

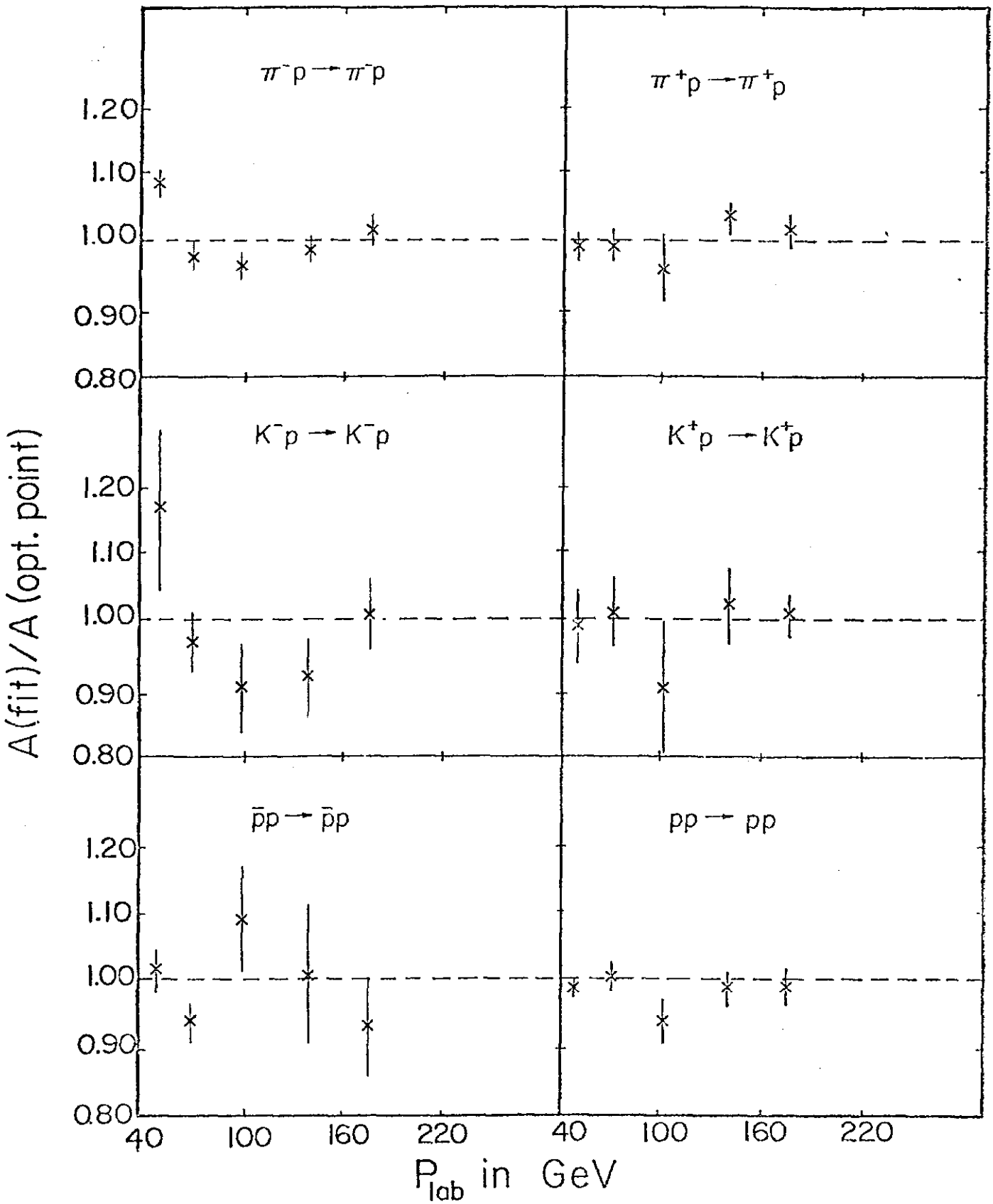
$\pi^- p \to \pi^- p$
$\pi^+ p \to \pi^+ p$
$K^- p \to K^- p$
$K^+ p \to K^+ p$
$\bar{p}p \to \bar{p}p$
$pp \to pp$
A(fit)/A (opt. point)
1.20
1.10
1.00
0.90
0.80
40
100
160
220
P_{lab} in GeV

FIGURE 1

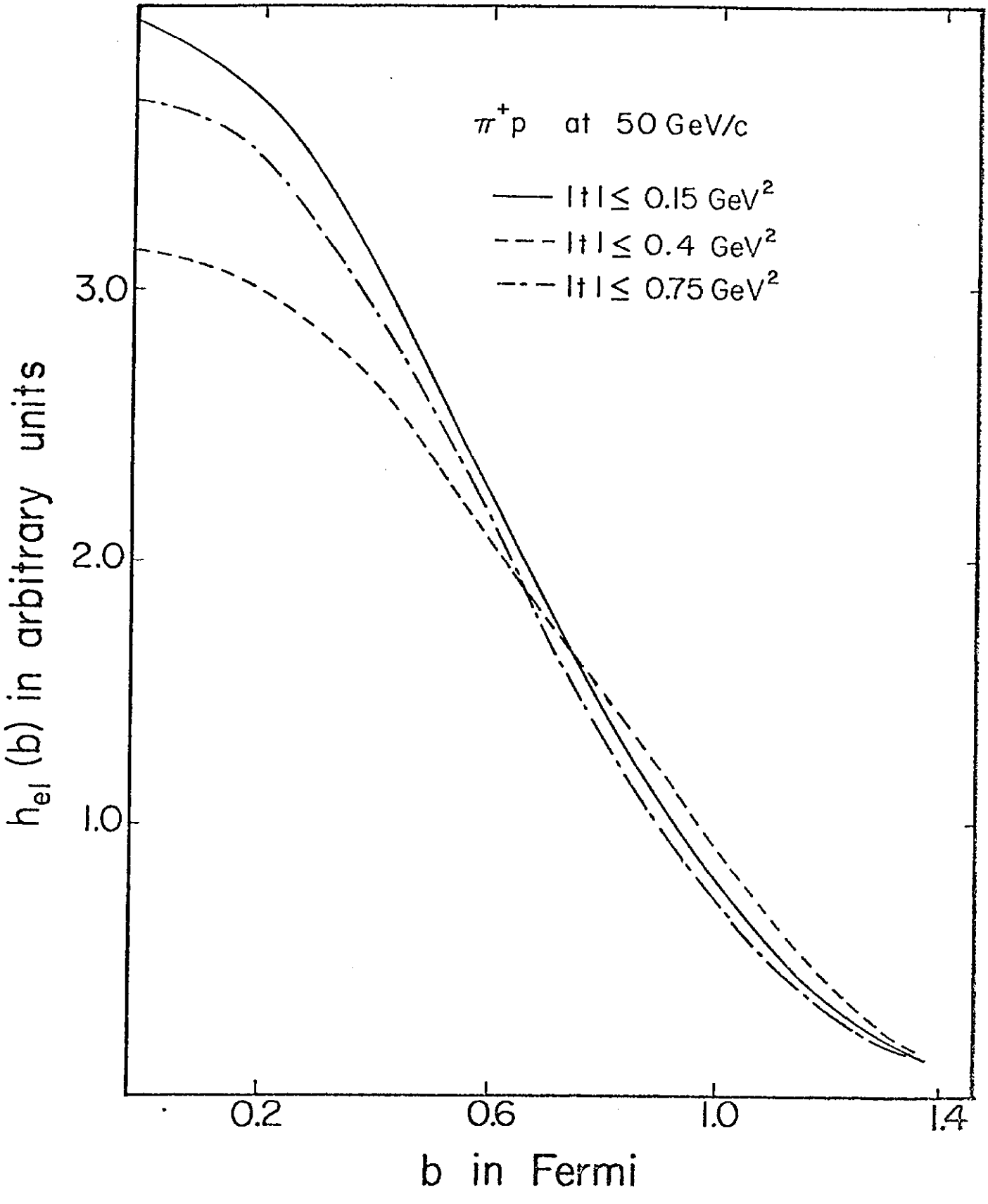
$\pi^+ p$ at 50 GeV/c
$|t| \leq 0.15$ GeV^2
$|t| \leq 0.4$ GeV^2
$|t| \leq 0.75$ GeV^2
$h_{el}(b)$ in arbitrary units
3.0
2.0
1.0
0.2
0.6
1.0
1.4
b in Fermi

FIGURE 2

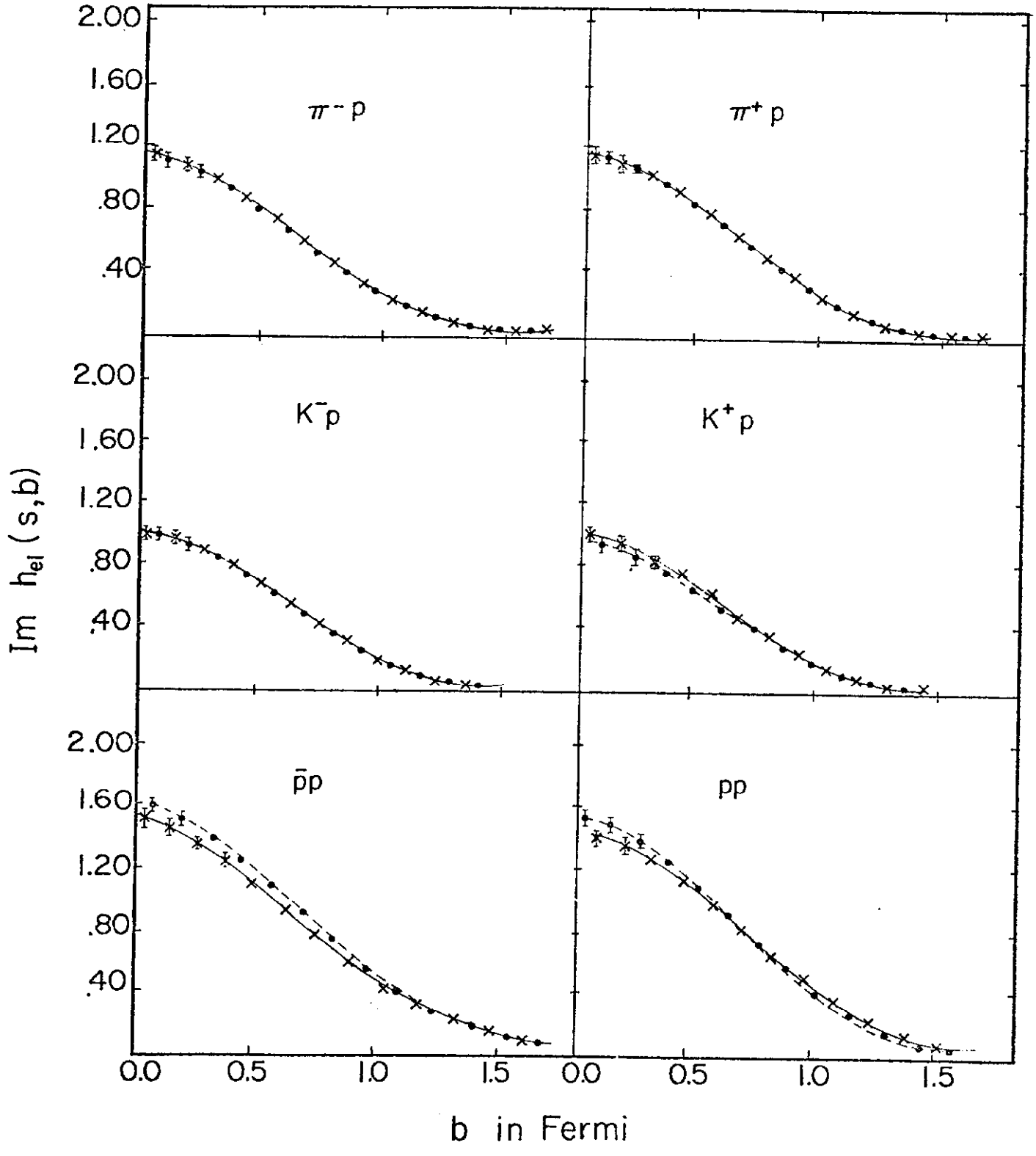
2.00
1.60
1.20
.80
.40
$\pi^- p$
$\pi^+ p$
$K^- p$
$K^+ p$
$\bar{p}p$
pp
0.0
0.5
1.0
1.5
Im $h_{el}(s,b)$
b in Fermi

FIGURE 3

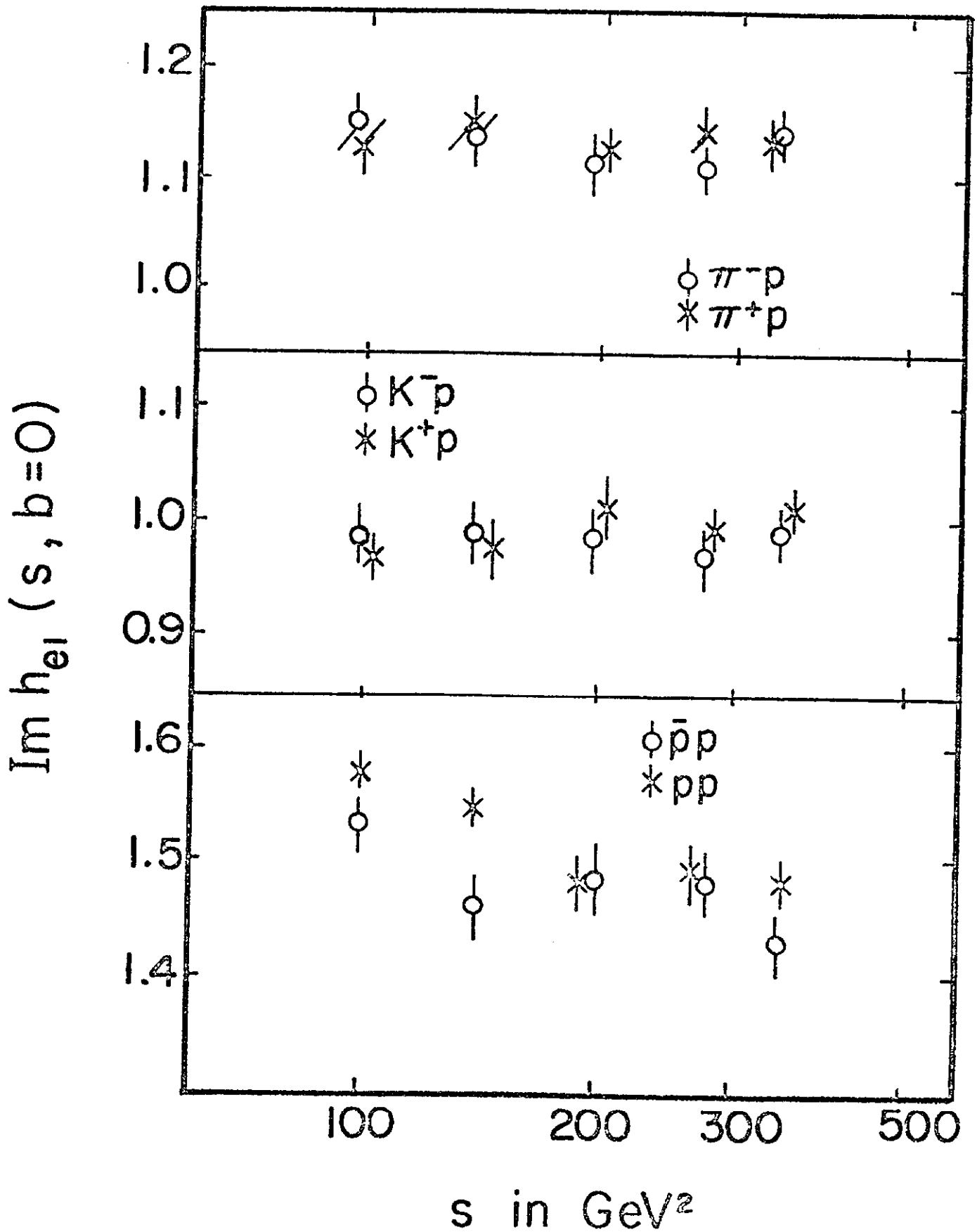
1.2
1.1
1.0
1.1
1.0
0.9
1.6
1.5
1.4
$\pi^- p$
$\pi^+ p$
$K^- p$
$K^+ p$
$\bar{p} p$
pp
100
200
300
500
Im h_{el} (s, b=0)
s in GeV^2

FIGURE 4

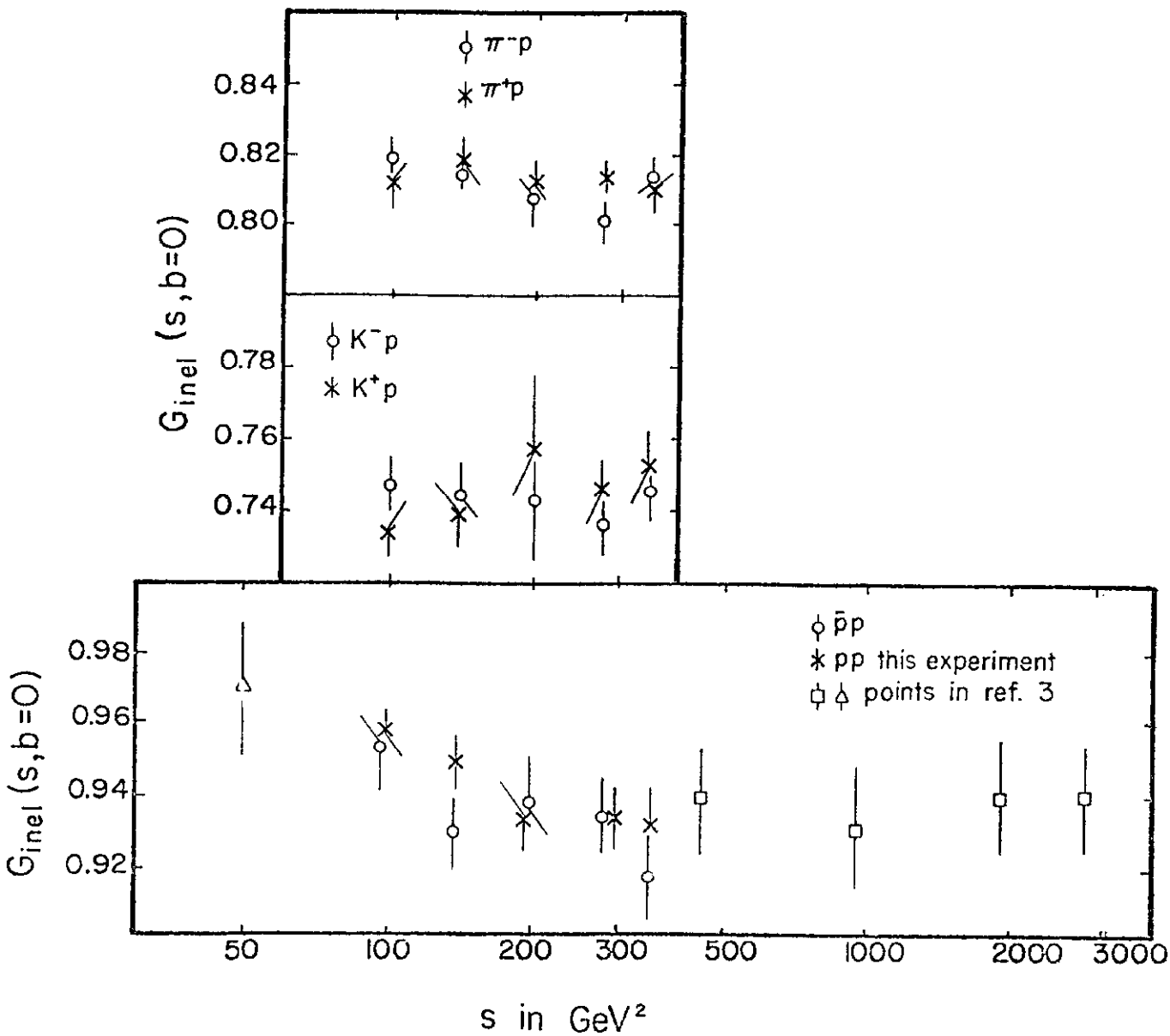
π^-p
π^+p
K^-p
K^+p
$\bar{p}p$
pp this experiment
points in ref. 3
$G_{inel}(s,b=0)$
0.84
0.82
0.80
0.78
0.76
0.74
0.98
0.96
0.94
0.92
50
100
200
300
500
1000
2000
3000
s in GeV²

FIGURE 5

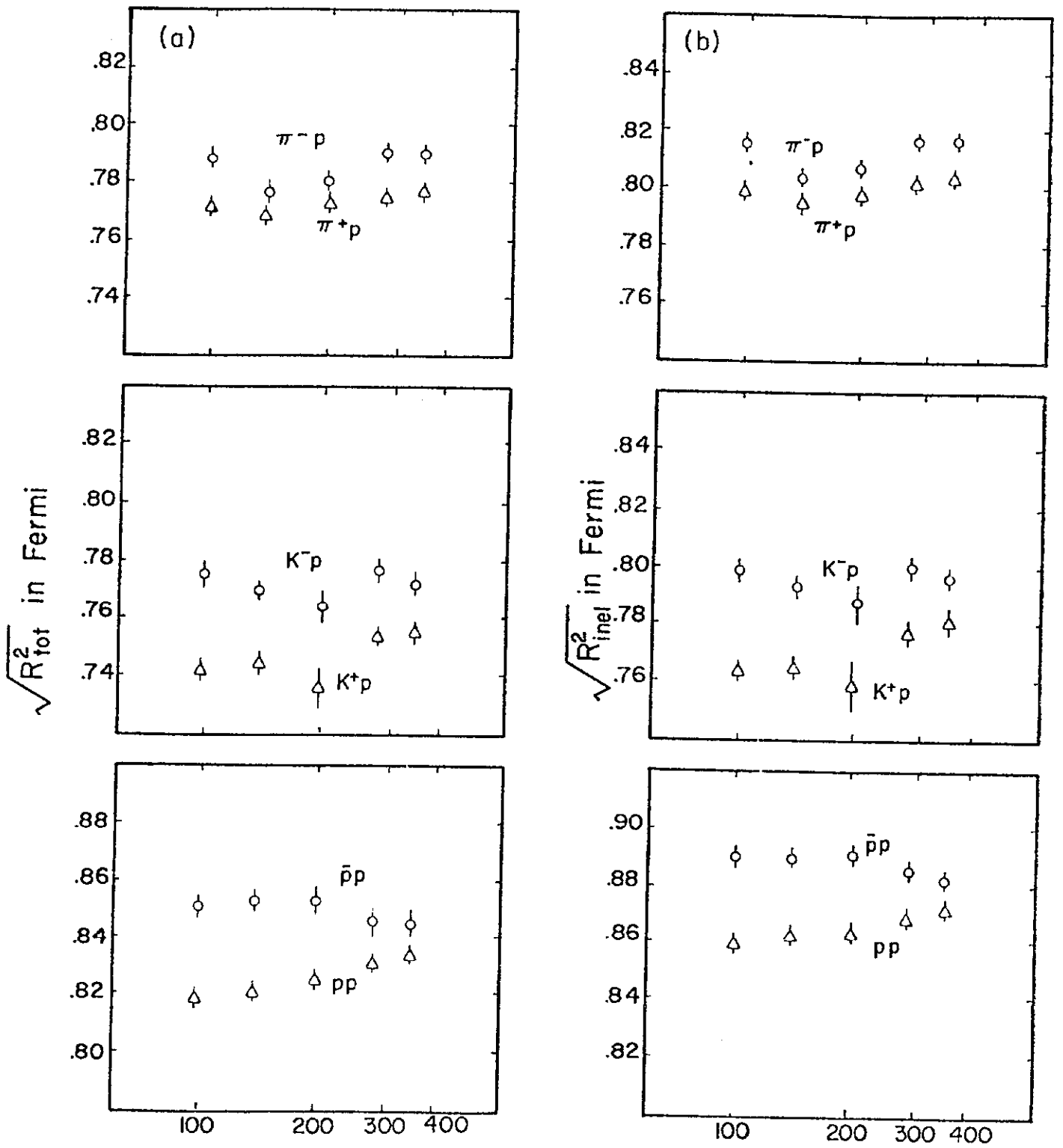
(a)
(b)
$\pi^- p$
$\pi^+ p$
$K^- p$
$K^+ p$
$\bar{p}p$
pp
$\sqrt{R^2_{tot}}$ in Fermi
$\sqrt{R^2_{inel}}$ in Fermi
S in GeV^2

FIGURE 6

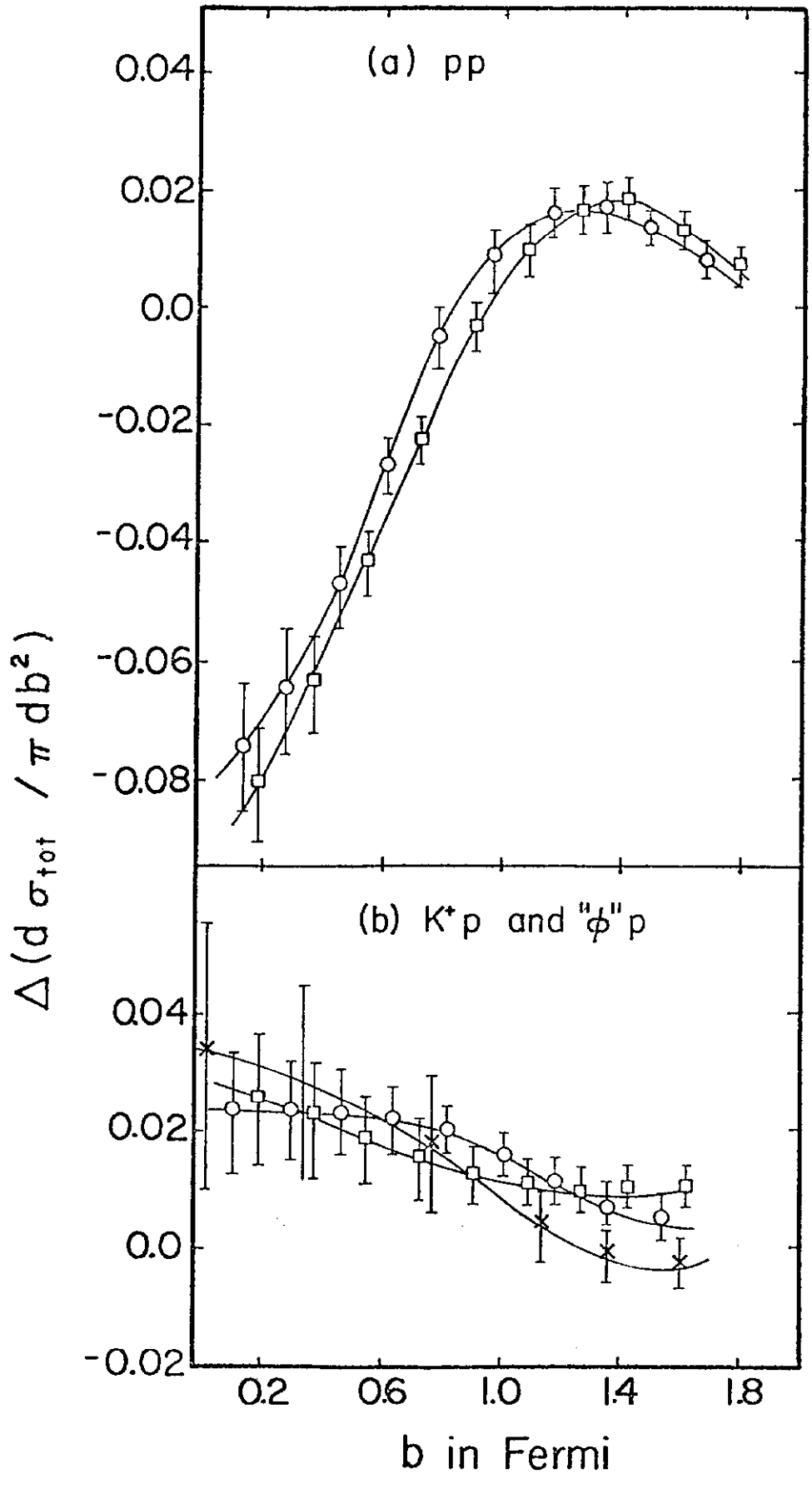
(a) pp
(b) K⁺p and "φ"p
0.04
0.02
0.0
-0.02
-0.04
-0.06
-0.08
0.04
0.02
0.0
-0.02
0.2
0.6
1.0
1.4
1.8
b in Fermi
Δ(d σtot / π db²)

FIGURE 7

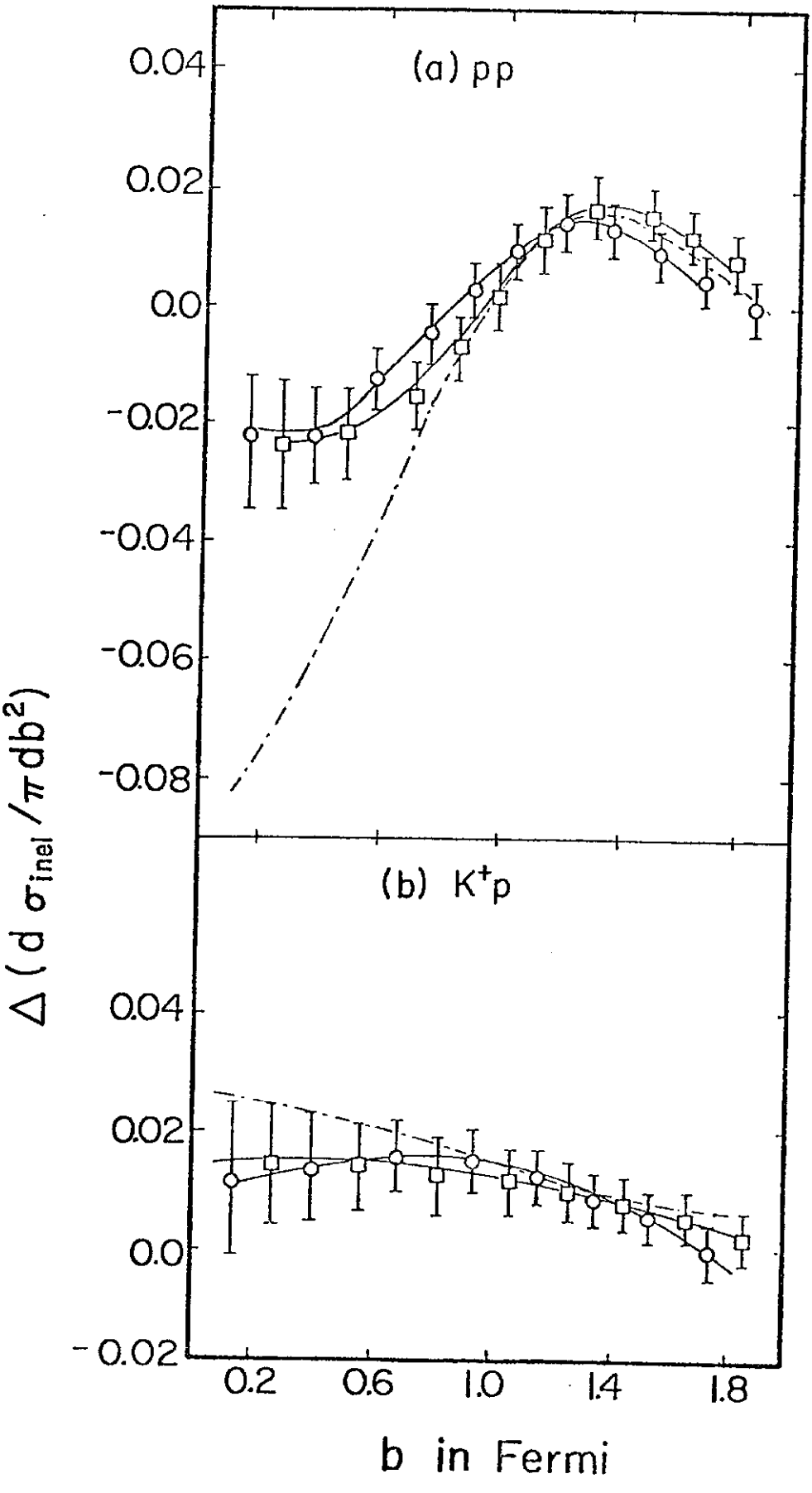
(a) pp
(b) K⁺p
0.04
0.02
0.0
-0.02
-0.04
-0.06
-0.08
0.04
0.02
0.0
-0.02
0.2
0.6
1.0
1.4
1.8
Δ (d σ inel / π db²)
b in Fermi

FIGURE 8

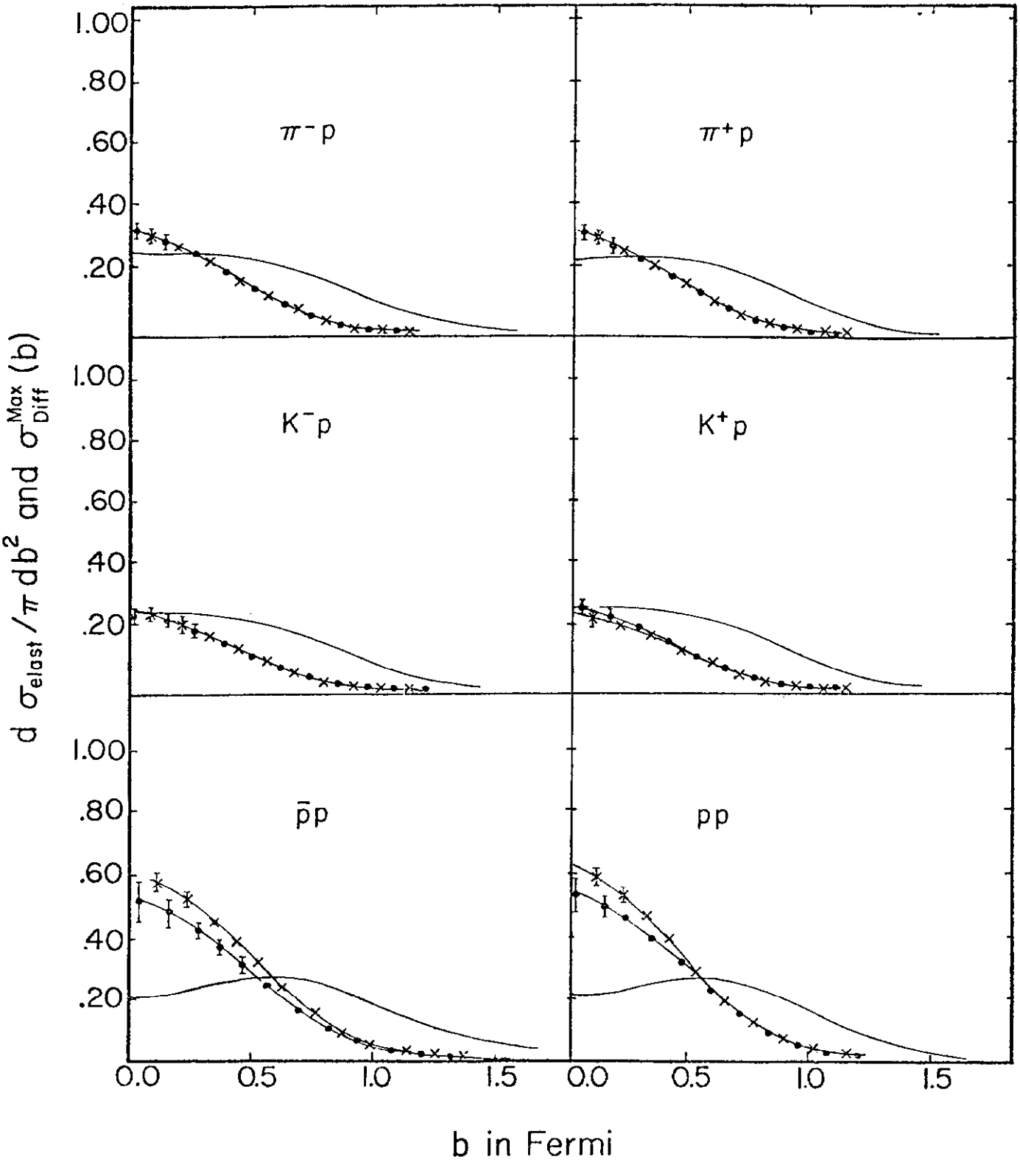
1.00
.80
.60
.40
.20
$\pi^- p$
$\pi^+ p$
$K^- p$
$K^+ p$
$\bar{p}p$
pp
0.0
0.5
1.0
1.5
d σ_{elast} / π db^2 and σ_{Diff}^{Max} (b)
b in Fermi

FIGURE 9

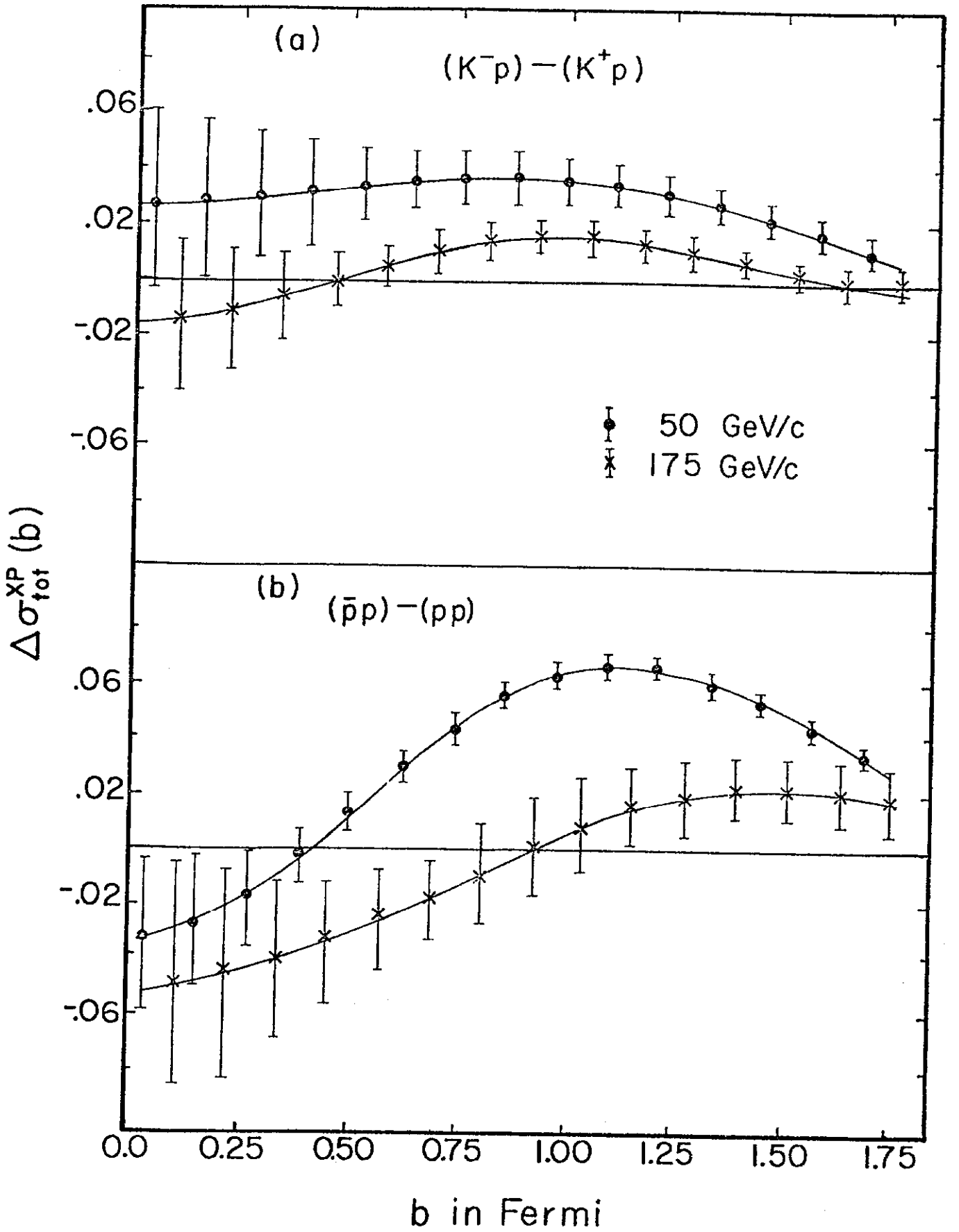
(a)
$(K^-p)-(K^+p)$
.06
.02
-.02
-.06
50 GeV/c
175 GeV/c
(b)
$(\bar{p}p)-(pp)$
.06
.02
-.02
-.06
$\Delta\sigma_{tot}^{XP}$ (b)
0.0
0.25
0.50
0.75
1.00
1.25
1.50
1.75
b in Fermi

FIGURE 10

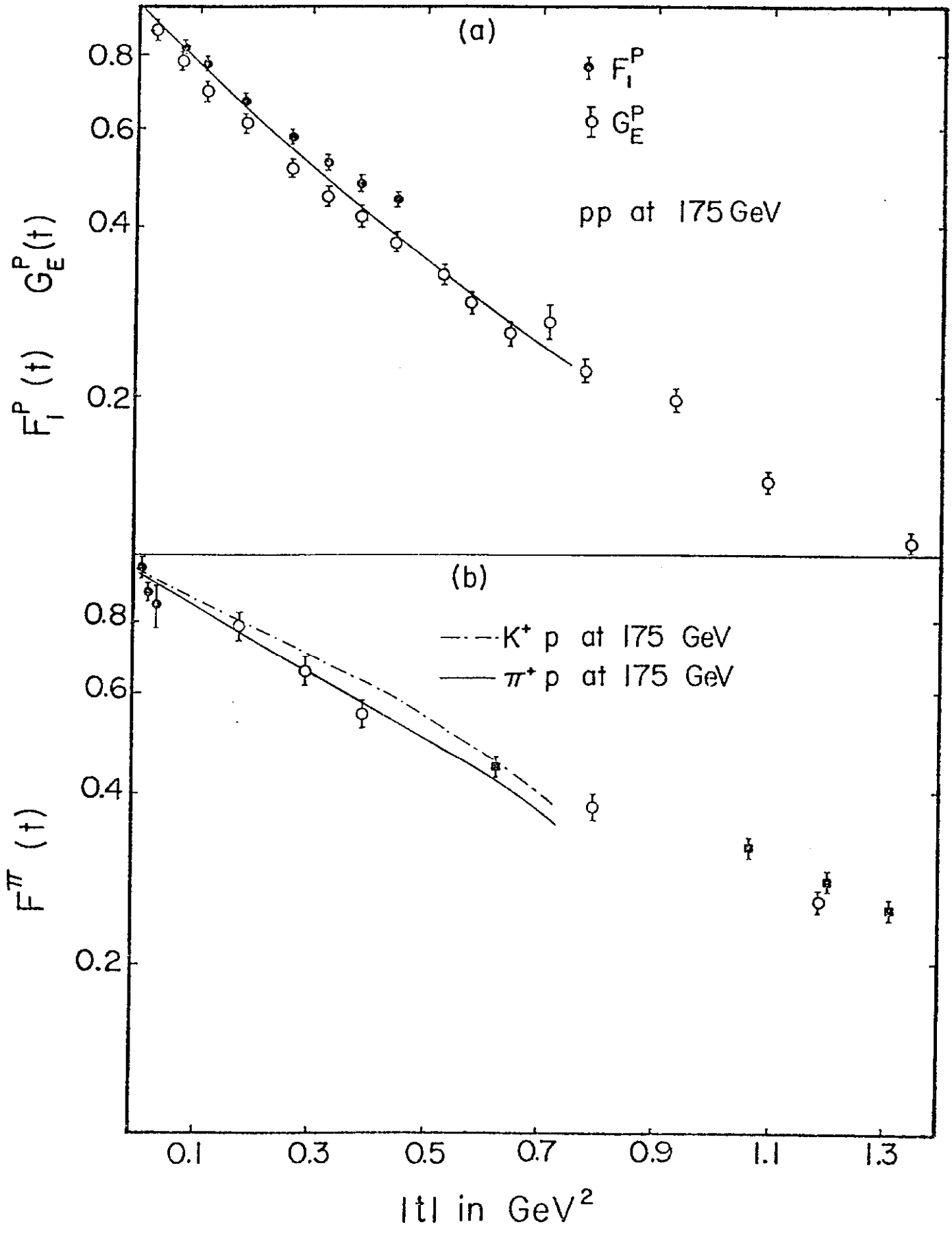
(a)
F_1^P
G_E^P
pp at 175 GeV
$F_1^P(t)$ $G_E^P(t)$
0.8
0.6
0.4
0.2
(b)
K^+ p at 175 GeV
π^+ p at 175 GeV
$F^{\pi}(t)$
0.8
0.6
0.4
0.2
0.1
0.3
0.5
0.7
0.9
1.1
1.3
|t| in GeV^2

FIGURE 11

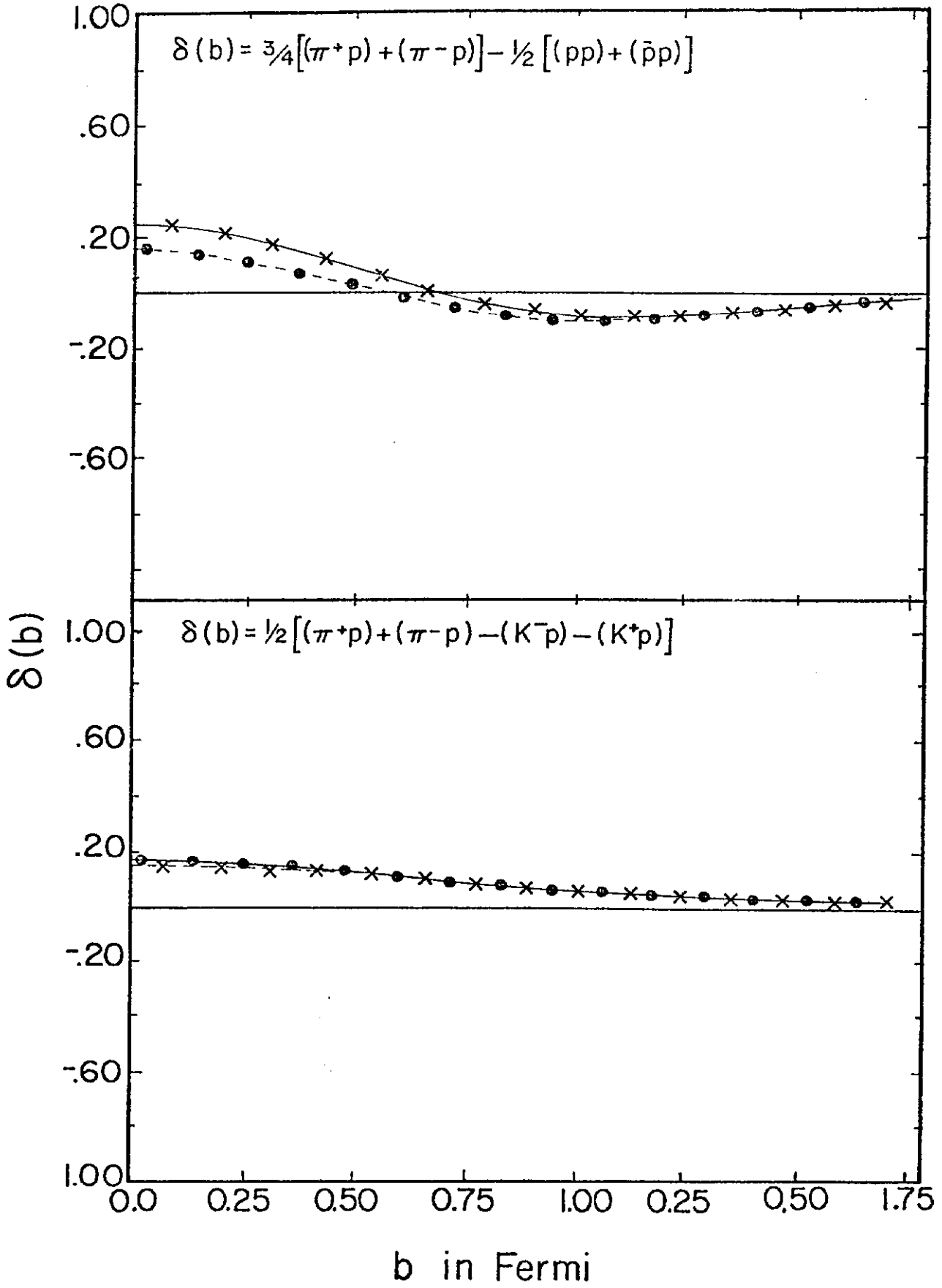
δ(b) = ¾[(π⁺p) + (π⁻p)] − ½[(pp) + (p̄p)]
δ(b) = ½[(π⁺p) + (π⁻p) − (K⁻p) − (K⁺p)]
δ(b)
1.00
.60
.20
-.20
-.60
1.00
.60
.20
-.20
-.60
1.00
0.0
0.25
0.50
0.75
1.00
0.25
0.50
1.75
b in Fermi

FIGURE 12

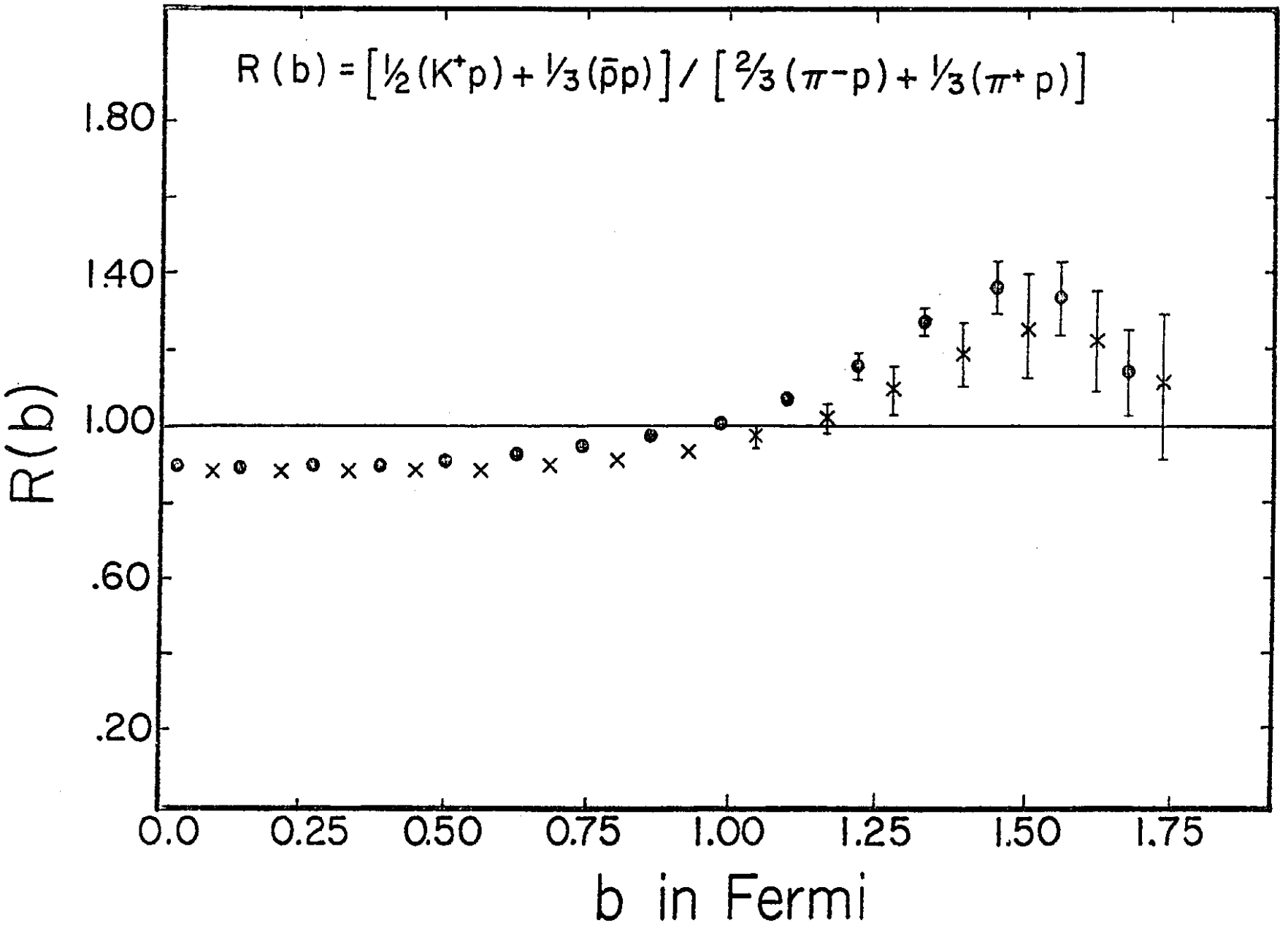
R (b) = [½ (K⁺p) + ⅓ (p̄p)] / [⅔ (π⁻p) + ⅓ (π⁺p)]
1.80
1.40
1.00
.60
.20
R(b)
0.0
0.25
0.50
0.75
1.00
1.25
1.50
1.75
b in Fermi